

# Results of first experiments with fusion targets at the Iskra-5 high-power laser installation

A. V. Bessarab, V. A. Gaïdash, G. V. Dolgoleva, N. V. Zhidkov, V. M. Izgorodin, G. A. Kirillov, G. G. Kochemasov, A. V. Kunin, D. N. Litvin, V. M. Murugov, G. F. Nasyrov, V. T. Punin, V. G. Rogachev, A. V. Senik, N. A. Suslov, G. V. Tachaev, and V. I. Shemyakin

*All-Union Scientific-Research Institute of Experimental Physics, Arzamas 16, Nizhniï Novgorod Oblast, USSR*

(Submitted 12 March 1992)

*Zh. Eksp. Teor. Fiz.* **102**, 1800–1807 (December 1992)

The first experiments with fusion targets have been carried out at the high-power, 12-channel Iskra-5 iodine laser at the All-Union Scientific-Research Institute of Experimental Physics. The laser output energy was about 12 kJ at a pulse length of 0.25 ns and a beam divergence of less than  $10^{-4}$  rad. A technique has been developed for fabricating thin-walled fusion targets for internal deposition of the laser light (inverted-corona targets). A yield of  $5 \times 10^9$  D–D neutrons was achieved with targets using deuterated polyethylene as working medium. The measured plasma ion temperature ranges up to 7 keV. The experimental results agree satisfactorily with theoretical predictions.

## INTRODUCTION

The basic task in the effort on laser controlled fusion today is to determine the laser parameters and the types of targets which will make it possible to ignite the fusion fuel. The existing facilities do not have an energy sufficient to achieve ignition. They are being used for a comprehensive study of the physics of targets and to build up the experimental database necessary for selecting the best way to solve the laser fusion problem.

Targets can be divided into two categories on the basis of the method by which the laser light is applied: external-heating targets (Refs. 1 and 2, for example) and internal-heating targets (Refs. 3–5, for example). The simplest internal-heating target is the inverted-corona target. The operation of this target was studied previously with the Iskra-4 laser.<sup>5</sup> Targets of this type have a high energy utilization factor and impose relatively relaxed requirements on the uniformity of the light. They are intended for use in research on nonequilibrium processes in hot plasmas.

In the inverted-corona target, the efficiency with which energy is transferred to the ions of the fusion plasma is exceptionally high, and a substantial difference between the electron and ion temperatures develops. When laser light with an energy of 1–10 kJ is delivered to the target, the plasma ions can be heated to 3–10 keV, and a significant neutron yield can be obtained.

Once we have reached an understanding of the physics of an inverted-corona target and of the processes accompanying the input of light into the target cavity, we will be in a position to move on to studies of targets of more complex design, e.g., the Cannonball.<sup>3</sup>

The efficiency with which the laser light is injected into the target depends on how the apertures are covered by the expanding plasma. It also increases with decreasing pulse length. The comparatively short pulses of the Iskra-4 and Iskra-5 lasers thus make these devices convenient tools for studying the operation of internal-heating targets.

Previous experiments with inverted-corona targets using deuterated polyethylene as working medium<sup>5</sup> have succeeded in producing more than  $10^7$  D–D neutrons at a laser

energy of about 0.5 kJ. In the present paper we are reporting the first results on inverted-corona targets at laser energies up to 10 kJ.

## THE LASER FACILITY

The Iskra-5 high-power iodine photodissociation laser is a 12-channel system with series-parallel amplification of light at the wavelength  $\lambda = 1.315 \mu\text{m}$ .

A single pulse 0.5 ns long is formed by a laser oscillator with active mode locking. After the light emerges from the preliminary amplification stages, it is broken up into 12 channels by a system of beam splitters. There are five amplification stages in each channel, with a progressively increasing aperture. The angular distribution of the light is shaped, and self-excitation is avoided by separating the various stages by spatial filters and phototropic brightening shutters. The diameter of the output beam is 680 mm.

The energy of the light emerging from each channel ranges up to 2.5 kJ, in a pulse 0.25 ns long, with an angular divergence of less than  $10^{-4}$  rad. The energy contrast and power contrast of the laser pulse are both greater than  $10^6$ .

The Iskra-5 has an evacuated target chamber 2200 mm in diameter. The light is focused on the target by 12 mirror-lens objectives with a speed of 1:1.6. The Iskra-5 and its characteristics are described in detail in Ref. 6.

## THE TARGET

The inverted-corona target used in these first experiments was a spherical copper shell 2 mm in diameter and 5  $\mu\text{m}$  thick. A layer of deuterated polyethylene  $(\text{CD}_2)_n$ , about 1  $\mu\text{m}$  thick was deposited on the inner surface of the shell.

The light entered the target through six apertures 600  $\mu\text{m}$  in diameter; two beams go through each aperture (Fig. 1). The foci of the objectives coincide with the centers of these apertures. The angular coordinates of the centers of the apertures and the beam entry directions were chosen to maximize the uniformity with which the inner surface was irradiated.

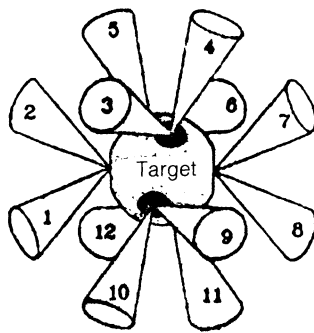


FIG. 1. Entry of the laser beams into the inverted-corona target. 1–12—laser beams.

### EXPERIMENTAL RESULTS

The experimental results are summarized in Table I, where  $E_t$  is the energy of the light delivered to the target,  $E_s$  is the loss of radiant energy as the result of reflection and scattering,  $E_{ab}$  is the absorbed energy,  $T_i$  is the effective ion temperature of the fusion plasma, and  $N_{DD}$  is the total yield of 2.45-MeV neutrons.

The energy of the light was measured in each of the 12 channels. For this purpose, part of the beam energy ( $\leq 1\%$ ) was tapped from the entire beam aperture and sent to a measurement line, where it was focused on TPI-2A calorimeters. The total energy delivered to the target was found by summing the energies measured in the various channels and correcting for the transmission of the focusing optics ( $k \approx 0.75$ ). The overall error in the determination of  $E_t$  was less than 20%.

The energy  $E_s$ , representing the light which reflected from the plasma and refracted by the plasma corona (and which escaped through the apertures), was measured by special calorimeters like those of Ref. 7. The sensitive areas of these calorimeters were made of NS-12 glass, with a high absorption coefficient at the laser wavelength. The temperature sensors were TMO-8 semiconductor thermocouples. Filters of BS-8 glass, which is transparent for the laser light, were used to protect the sensitive area from the radiation emitted by the plasma (in the UV and x-ray ranges).

The absorbed energy  $E_{ab}$ , as the sum of the kinetic energy of the plasma and the radiation emitted by the plasma over the wavelength range 1–3000 Å, was measured with special calorimeters like those of Ref. 8. The sensitive area of these calorimeters was made of BS-8 glass, in contrast with that of the calorimeters used to measure the energy of the laser light.

The calorimeters used to measure  $E_s$  and  $E_{ab}$  were structurally a single measurement module. Four–six of these modules were positioned 1 m from the target to measure the

energy flux in various radial directions.

Table I lists average values of  $E_s$  and  $E_{ab}$  found from the calorimetric measurements under the assumption that the energy flux from the target is isotropic. Also shown here are the standard deviations of  $E_s$  and  $E_{ab}$ .

The energy balance ( $E_t = E_s + E_{ab}$ ) holds approximately when allowance is made for the errors in the measurements of all three of these energies. The greatest error is in the determination of  $E_s$  and  $E_{ab}$ , which are found by averaging the data from a relatively small number of calorimeters with allowance for the observed anisotropy of the energy flux. The absorbed energy can also be calculated as the difference between the energy delivered to the target and the energy of the scattered laser light:  $E_{ab}^* = E_t - E_s$ . In the interpretation of the experiments below we use the average value

$$Q_a = (E_{ab} + E_{ab}^*) / 2.$$

The total neutron yield was measured by an activation method and by a prolonged-detection method.<sup>9</sup> The silver-activation detector had a threshold of  $10^7$  neutrons, and the prolonged-detection detector had one of  $3 \times 10^6$  neutrons. The error in the measurements of the total neutron yield was due primarily to the error in the absolute calibration of the detectors in the real geometry of the experimental apparatus.

The effective ion temperature (averaged over the volume occupied by the hot plasma and also averaged over time) was found by the time-of-flight method<sup>9</sup> from the broadening of the neutron pulse over a baseline  $L \approx 11$ –12 m. The neutron pulse was detected by two scintillation detectors through a concrete collimator 10 cm in diameter and 140 cm long. The mass thickness of the chamber wall in the detection direction was 2.4 g/cm<sup>2</sup> of Fe plus 4.5 g/cm<sup>2</sup> of Pb. This thickness protected the detectors from the hard x radiation from the target without causing any significant distortion of the shape of the neutron pulse due to scattering.

Figure 2 shows a typical oscilloscope trace from the time-of-flight measurements. The center of the pulse (the delay in the triggering of the oscilloscope is taken into account here) agrees to within about 1 ns with the calculated arrival time of the D–D neutrons at the detector. The error in the measurements of the ion temperature was determined from the time resolution of the detector, the limited statistical base of detected neutrons, and the error in the analysis of the resulting oscillograms. Estimates showed that the baseline selected for the time-of-flight measurements is close to the optimum value at the maximum neutron yield detected, where the total error in the measurements of the ion temperature was less than  $\pm 15\%$ . When the neutron yield was about  $7 \cdot 10^8$  the error in the  $T_i$  measurements increased to

TABLE I.

N	$E_t$ , kJ	$E_s$ , kJ	$E_{ab}$ , kJ	$T_i$ , keV	$N_{DD}$
1	$0,2 \pm 0,04$	—	—	—	$(9 \pm 3) \cdot 10^8$
2	$1,3 \pm 0,3$	$0,3 \pm 0,2$	$0,35 \pm 0,15$	—	$(5 \pm 2) \cdot 10^8$
3	$2,3 \pm 0,5$	$0,6 \pm 0,4$	$0,8 \pm 0,4$	$4,0 \pm 2$	$(7 \pm 2) \cdot 10^8$
4	$7,3 \pm 1,5$	$2,3 \pm 0,8$	$3,1 \pm 0,4$	$7,5 \pm 1$	$(5 \pm 2) \cdot 10^9$
5	$9,0 \pm 1,8$	$2,5 \pm 0,3$	$4,4 \pm 0,8$	$7,5 \pm 1$	$(5 \pm 2) \cdot 10^9$

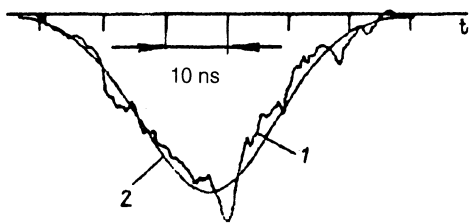


FIG. 2. Oscilloscope trace of the time-of-flight detection of the neutron pulse in experiment No. 5 ( $Q_{ab} \approx 5.5$  kJ). 1—Experimental; 2—theoretical for  $T_i = 8$  keV.

$\pm 50\%$  and was due primarily to the error in the analysis of the small-amplitude oscilloscope signal.

Figure 3 shows some x-ray images of the target recorded with a pinhole camera behind various filters. At an x-ray energy  $h\nu \approx 1.5$  keV the apertures for the entry of the laser beams, were uniformly irradiated and emission also came from the plasma burst ejected from these apertures. The central region of compressed plasma can be seen fairly clearly on the image recorded at an x-ray energy  $h\nu \approx 4.5$  keV. The diameter of this compressed region is about  $500 \mu\text{m}$ .

Figure 4 shows the results of numerical processing of an image of the inner region of the target recorded in x radiation ( $h\nu \approx 1.5$  keV). The plasma at the center of the target has a relatively high symmetry.

## DISCUSSION OF RESULTS

A quantitative description of the operation of the inverted-corona target was obtained by solving the one-dimensional equations of two-temperature radiation gas dynamics numerically (by the ADI method<sup>10</sup>). The electron and ion thermal conductivities, the ion viscosity, the limitations on the heat fluxes, the generation and transport of nonequilibrium x radiation (calculated in a quasidiffusion approximation), and the relaxation of the electron and ion temperatures were all taken into account. Kinetic coefficients were calculated assuming that the various components of the plasma were fully ionized. The transport of laser light was described in the quasisteady approximation by means of a "sphericized" model.

The operation of the inverted-corona target can be thought of as consisting of three stages.

First, the laser light is absorbed by the layer of working medium; the latter evaporates, and a hot plasma is produced. The processes which occur in this stage are similar to those which occur when a laser pulse of the same intensity and length is applied to a plane target, except that nearly all the energy of the laser light remains in the target.

In the second stage the plasma coasts toward the center of the target. The plasma cools down in this stage. Internal

energy is converted into kinetic energy. According to calculations, the mass velocity reaches  $v \approx (1-2) \cdot 10^8$  cm/s when the amount of radiant energy absorbed in  $Q_a \approx 10$  kJ.

In an electrically neutral plasma, the electrons and ions move at identical average velocities. Since the mass of an ion is much greater than that of an electron, the kinetic energy is carried primarily by the ions. The processes which occur in the second stage results in extremely efficient conversion of the absorbed radiant energy  $Q_{av}$  into ion kinetic energy (up to 60–70% of  $Q_{av}$  is converted).

In the third stage the plasma is focused and a hot plasma forms at the center of the target. The ion kinetic energy is efficiently converted into thermal energy, and the plasma is heated. The ion temperature  $T_i$  reaches 10–20 keV and becomes much higher (by about an order of magnitude) than the electron temperature  $T_e$ . The density of the central plasma formation, with a diameter of about  $500 \mu\text{m}$ , reaches  $\rho = 0.02$  g/cm<sup>3</sup>.

This difference between the ion and electron temperatures arises because the plasma ions and electrons exchange energy relatively slowly, primarily because of the low plasma density. This wide difference in temperatures has the consequence that the electron heat capacity of the plasma has only a minor influence on the ion temperature. Accordingly, chemical compounds which contain heavier elements along with hydrogen isotopes can be used as fusion fuel without a significant reduction of  $T_i$ . These heavier elements lead to rapid relaxation to thermodynamic equilibrium in the plasma ions and improve the gasdynamic approximation for the plasma motion. In addition, such compounds make it unnecessary to use cryogenic methods to prepare the solid layer of hydrogen isotopes.

A high ion temperature promotes intense fusion reactions and thus a significant neutron yield.

The neutron emission reaches a maximum intensity  $\approx 1$  ns after the laser light reaches its own maximum intensity (at  $Q_{ab} \approx 10$  kJ). The delay is a consequence of the time involved in focusing the fast plasma component at the center of the target ( $\Delta t \approx R_0/v \approx 1$  ns). The neutron emission pulse lasts less than 1 ns.

Later on, the plasma expands and cools, and the electron and ion temperatures become equal. The fusion reaches essentially come to a halt, as does the neutron emission.

Figure 5 shows spatial distributions of the ion and electron temperatures calculated by the ADI method.

The calculated dependence of the neutron yield on the target size and the parameters of the laser light for  $Q_{ab} < 1$  kJ is interpolated with the help of the scaling law

$$N_{DD} \approx Q_a^{2.7} R_0^{2.7} \tau^{-0.65} = \left( \frac{Q_a}{R_0 \tau^{0.24}} \right)^{2.7} = D^{2.7}.$$

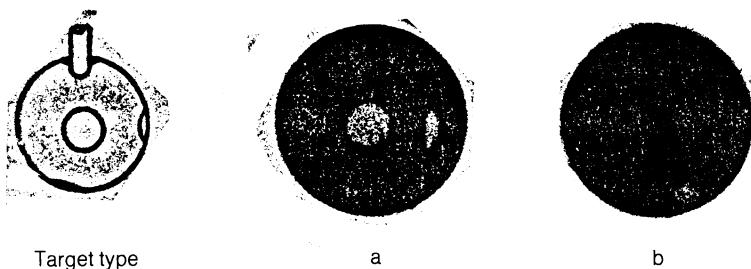


FIG. 3. X-ray images of the target. a— $h\nu \approx 1.5$  keV. Plasma bursts emerging from the apertures can be seen at the periphery of the target. b— $h\nu \approx 4.5$  keV. Only the central, inner part of the target can be seen.

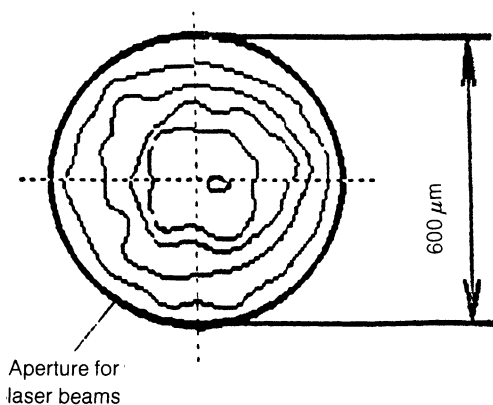


FIG. 4. Contour map of the  $x$  radiation from the central region of the plasma of the inverted-corona target in experiment No. 5.

In the interval  $1 \text{ kJ} < Q_{ab} < 20 \text{ kJ}$  we have  $N_{DD} \propto Q_{ab}^\alpha$ , where  $\alpha \approx 1.5-2$ .

Figure 6 shows the neutron yield from inverted-corona targets with polyethylene as working medium as a function of the quantity  $D = Q_{ab} / (R_0 t^{0.24})$ , where  $Q_{ab}$  is in kilojoules,  $R_0$  in millimeters, and  $\tau$  in nanoseconds. Shown for comparison is the scaling law  $N \propto D^{2.7}$ . The experimental points obtained earlier in Iskra-4 were taken from Ref. 5.

On the average, the discrepancy between the experimental data on  $N_{DD}$  and the results of the one-dimensional calculations is less than a factor of ten. This agreement can be viewed as satisfactory. Possible reasons why the experimental neutron yield is lower than the theoretical value are the deviation of the actual flow from spherical symmetry and the deviation of the composition of the working medium from  $(\text{CD}_2)_n$  because of impurities. Rough calculations based on numerical solution of the two-dimensional gasdynamic equations show that, at the prevailing degree of asymmetry ( $\approx 2$ ) in the irradiation of the inner surface of the

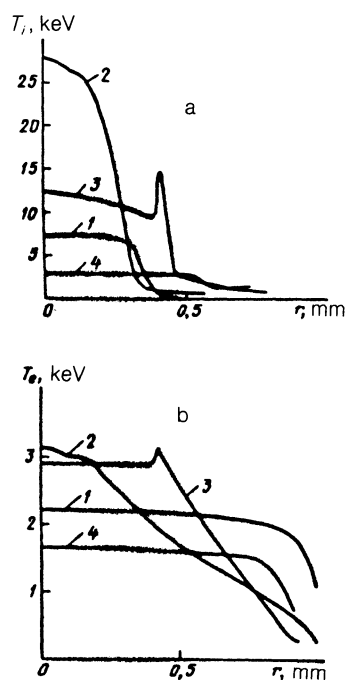


FIG. 5. Temperature distributions in the inverted-corona target. a—ion temperature; b—electron temperature.  $Q_{ab} = 6 \text{ kJ}$ ,  $\tau = 0.3 \text{ ns}$ ,  $R_0 = 1 \text{ mm}$ , 1—1 ns; 2—1.4; 3—1.8; 4—2.8 ns.

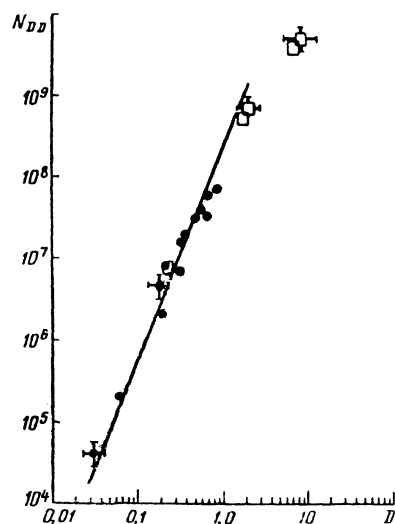


FIG. 6. Neutron yield from inverted-corona targets. ●—Iskra-4; □—Iskra-5; line—theoretical scaling,  $N_{DD} \approx D^{2.7}$ .

inverted-corona target, the neutron yield should be reduced by a factor of two or three.

Among the physical factors which were ignored in the calculations and which tend to reduce the neutron yield we should mention the spatial separation of ions of different species which results from their relative diffusion. This should be a significant effect, since the mean free paths of the deuterium and carbon ions with respect to collisions in the hot, low-density plasma of the inverted-corona target are comparable to the size of the plasma.

## CONCLUSION

The first experiments on the application of laser pulses with an energy up to 10 kJ to an inverted-corona target have been reported. A yield of  $5 \cdot 10^9$  D-D neutrons has been obtained with targets using deuterated polyethylene as working material. The measured plasma ion temperature reaches 10 keV. The experimental results agree satisfactorily with theoretical predictions found by analytical and numerical methods. Calculations show that switching to a working material containing equimolar amounts of deuterium and tritium would raise the neutron yield by a factor of about 70 (these would be D-T neutrons).

A study of the nonequilibrium processes which accompany the operation of an inverted-corona target will yield the physical information which we need on the properties of the hot plasma and will set the stage for moving on to targets of more complex construction, designed for achieving ignition.

<sup>1</sup>R. L. McCrory, I. M. Soares, C. P. Verdon *et al.*, *Nature* **335**, 255 (1988).

<sup>2</sup>H. Takabe, M. Yamanaka, K. Mima *et al.*, *Phys. Fluids* **31**, 2884 (1988).

<sup>3</sup>C. Nakai, *Nucl. Fusion* **30**, 1779 (1990).

<sup>4</sup>W. J. Hogan, *Fus. Eng. Design* **9**, 401 (1989).

<sup>5</sup>A. V. Bessarab, G. V. Dolgoleva, A. I. Zaretskii *et al.*, *Dokl. Akad. Nauk SSSR* **282**, 857 (1985) [*Sov. Phys. Dokl.* **30**, 478 (1985)].

<sup>6</sup>V. I. Annenkov, V. A. Bagretsov, V. G. Bezuglov *et al.*, *Kvant. Elektron.* (Moscow) **18**, 536 (1991) [*Sov. J. Quantum Electron.* **1**, 487 (1991)].

<sup>7</sup>Gann, *Rugyars*, *Rev. Sci. Instrum.*, No. 11, (1977).

<sup>8</sup>T. Ukida, Tanaka, Saseva *et al.*, *Rev. Sci. Instrum.*, No. 19, (1985).

<sup>9</sup>A. I. Veretennikov, V. M. Torbolev, and B. A. Predein, *Methods for Studying Pulsed Radiation*, Energoatomizdat, Moscow (1985).

<sup>10</sup>G. V. Dolgoleva, *VANT*, No. 2(13), 29 (1983), *Ser. Metodiki i programmy chislennogo resheniya zadach matematicheskoi fiziki*.

Translated by D. Parsons